Study of the radiation damage caused by ion implantation in ZnO and its relation to magnetism

Miaomiao Yuan[1], Xia Zhang[1], Ahmad M.A.Saeedi[2], Wei Cheng[1,3], Chungang Guo[1,3], Bin Liao[1,3], Xu Zhang[1,3], Minju Ying[1,3*], Gillian A. Gehring[2*]

1 Key Laboratory of Beam Technology of Ministry of Education, College of Nuclear Science and Technology, Beijing Normal University, Beijing 100875, China
2 Department of Physics and Astronomy, Hicks Building, University of Sheffield, Sheffield S3 7RH, United Kingdom
3 Beijing Radiation Center, Beijing 100875, China

[*] Address correspondence to E-mail: mjying@bnu.edu.cn , g.gehring@sheffield.ac.uk

Abstract

Multi-energy ion implantation has been employed to introduce different concentrations of non-magnetic ions, including argon, arsenic and krypton, into high-quality ZnO films and room temperature ferromagnetism has been observed for As and Kr implanted ZnO while none was observed for Ar doped films. SRIM was adopted to simulate the distributions of the implanted ions, the induced zinc and oxygen vacancies and the resulting interstitials. The atomic displacements per atom (dpa) was calculated to quantify the primary radiation damage production. Our results show that the observed magnetic moment measured at low temperatures due to implantation with a given ion is proportional to the dpa. The constant of proportionality between the magnetism and the dpa depends on the implanted ion. This constant is largest for heavy, large ions. To obtain room temperature d^0 magnetism in ZnO, non-magnetic ions with high mass are suggested to be implanted into ZnO films.

Keywords: Ion implantation, d^0 magnetism , ZnO, RT ferromagnetism, defects

1. Introduction

The processing and transmission of information based on semiconductors currently only uses the charge degree freedom of the electrons. Meanwhile, the storage of information based on magnetic materials only uses the spin degree of freedom of the electrons [1]. It will bring great breakthroughs to information technology if the electrons' spin and charge degrees of freedom can be controlled simultaneously, this is known as spintronics. Diluted magnetic semiconductors (DMSs) are an example of a material which can show both semiconducting and magnetic properties. Since the theoretical prediction of a possible room temperature ferromagnetism in Mn-doped ZnO [2], ZnO-based dilute magnetic semiconductors have attracted much attention over the past decade due to their potential applications in spintronic devices. Many studies have shown that the inclusion of 3d transition metal dopants in ZnO leads to ferromagnetism at room temperature. The 3d transition metal ions contain unpaired electrons which can provide the magnetic dipole moments [3-6].

In recent years ferromagnetism has also been achieved in ZnO which was either un-doped or doped with a nonmagnetic ion [7, 8]. This is known as d^0 ferromagnetism. It has been found that d^0 ferromagnetism is strongly correlated with low crystalline quality because defects play an important role in establishing the long-range ferromagnetism [9-11]. However, the origin of the magnetism remains controversial as it may be due to particular point defects or to the regions in the grain boundaries.

In this paper, high quality ZnO films have been prepared by rf-plasma assisted molecular beam epitaxy on sapphire substrates and ion implantation has been adopted to introduce non-magnetic ions into these films in order to assess the effects of defects on magnetism. Ion implantation is a nonequilibrium and reproducible approach to introduce doped elements and defects into crystalline materials. Accelerated ions will leave a trail of atoms displaced from their equilibrium lattice sites, thus creating vacancies, interstitials or antisites before they finally come to rest and become a nonmagnetic dopant. Single energy ion implantation has a near Gaussian distribution and in our experiments, a sequence of four implantation energies was used to produce a nearly box-like distribution of doped ions throughout a given depth in the films. The

evolution of structure, optical and magnetic properties for As and Kr implanted ZnO films has been studied experimentally [12,13]. To study the effects of ion mass on magnetization, multi-energy Ar implantation has been carried out to introduce similar concentrations of Ar as Kr but no magnetism was observed for Ar doped ZnO films. In this paper, we used the Monte Carlo simulation code named Stopping and Range of Ions in Materials (SRIM) to simulate the distributions of the multi energy implanted ions and the implantation induced zinc and oxygen vacancies and interstitials. A common radiation damage parameter, known as atomic displacements per atom (dpa), which is defined as the average number of displacements per atom in the target produced by a given radiation fluence, was calculated to serve as a standard measure of primary radiation damage production. Our results show that the observed magnetic moment measured at low temperatures due to implantation with a given ion is proportional to the dpa. The constant of proportionality between the magnetism and the dpa depends on the implanted ion. This constant is largest for heavy, large ions. This may because ions with a large mass and radius implanted into the grains may cause a marked grain fragmentation, leading to an increase in the volume of the sample occupied by grain boundaries [13]. Although the dpa is commonly used as a quantitative measure of radiation damage, and ion implantation induced d^0 magnetism has often been observed experimentally, there are currently no reports on the results of a study of the relationship between the value of the dpa and the magnitude of magnetism for ions implanted into ZnO films. This study is also the first to investigate the effects of the mass of the implanted ions on the dap and magnetism.

2. Experimental details

A RF plasma-assisted molecular beam epitaxy (MBE) system was used to grow high quality O-polar ZnO films of 300-400 nm on sapphire substrates [11,13]. The c plane of sapphire substrates were exposed to an oxygen plasma (270 W/1.5 sccm) at 500 ℃ for 30min to obtain a uniform oxygen terminated surface. After that, a thin

Table 1 The implantation parameters and magnetization for samples 1 to 9.

Samples	ions	Energies (keV)	Fluence (cm^{-2})	Concentration (cm^{-3})	Magnetization (emu/cm^{-3})		Maximum dpa
					5K	300K	
Sample 1	As	400 200 100 30	1×10^{13} 3×10^{12} 2×10^{12} 1×10^{12}	8×10^{17}	0 ± 10	0 ± 10	0.0254
Sample 2	As	400 200 100 30	1×10^{14} 3×10^{13} 2×10^{13} 1×10^{13}	8×10^{18}	4 ± 10	2 ± 10	0.254
Sample 3	As	400 200 100 30	1×10^{15} 3×10^{14} 2×10^{14} 1×10^{14}	8×10^{19}	15 ± 10	14 ± 10	2.54
Sample 4	Kr	200 150 80 30	2.5×10^{14} 5×10^{13} 7.5×10^{13} 5×10^{13}	5×10^{19}	0 ± 10	0 ± 10	0.865
Sample 5	Kr	200 150 80 30	5×10^{14} 1×10^{14} 1.5×10^{14} 1×10^{14}	1×10^{20}	38 ± 10	28 ± 10	1.73
Sample 6	Kr	200 150 80 30	2.5×10^{15} 5×10^{14} 7.5×10^{14} 5×10^{14}	5×10^{20}	186 ± 10	185 ± 10	8.65
Sample 7	Ar	200 150 80 30	5×10^{14} 1.5×10^{14} 2.5×10^{14} 8×10^{13}	5×10^{19}	0 ± 10	0 ± 10	0.678
Sample 8	Ar	200 150 80 30	1×10^{15} 3×10^{14} 5×10^{14} 1.6×10^{14}	1×10^{20}	0 ± 10	0 ± 10	1.356
Sample 9	Ar	200 150 80 30	5×10^{15} 1.5×10^{15} 2.5×10^{15} 8×10^{14}	5×10^{20}	0 ± 10	0 ± 10	6.78

MgO buffer layer was prepared at 500 ℃, which was followed by a ZnO buffer layer and epilayer growth at 450 ℃ and 650 ℃ respectively. O-polar films were used because it is known that these films absorb impurities more readily [14]. Argon, arsenic and krypton ions were introduced into ZnO films using ion implantation. In order to get a uniform distribution of implanted ions near the film surface, we adopted a multi-energy implantation procedure at room temperature. A sequence of four energies (400keV, 200keV, 100keV, and 30keV for As, and 200keV, 150keV, 80keV, and 30keV for Ar and Kr) were used and three samples for each type of dopants with different concentrations were made. Sample 1 to sample 3 were doped with As ions, sample 4 to sample 6 were doped with Kr ions and sample 7-9 were implanted with Ar ions. Detailed ion implantation parameters (implantation energies, fulences, and concentrations) for all the samples are shown in Table 1. A superconducting quantum interference device (SQUID, Quantum Design, MPMS) magnetometer was employed to characterize the magnetic properties for all the samples at 5 K and 300 K and also unimplanted films so that background signal could be subtracted. The magnetization is measured in emu, M_0, in a film of area A, magnetization per unit volume is defined as $m = \frac{M_0}{Ad}$ emu/cm^3. Here d is the approximate thickness of the implanted region, which is obtained by the distributions of implanted ions by SRIM calculations. The magnetization for all the samples are also shown in Table 1.

3. Results and discussions

It is well known that defects play an important role in the observed magnetism of non-magnetic ions doped ZnO. Although structure characterizations have been carried out in many literatures to characterize the magnetic ZnO [11-13,15-17], it still remains difficult to have a precise experimentally characterization of point defects in the doped ZnO. SRIM was written to permit the calculation of ion deposition profiles in materials exposed to energetic beams of ions [18-21]. It can also be used to simulate the damage in the target due to implantation. In this paper, we used SRIM-2008 to simulate the distribution of implanted ions and implantation induced damage in Ar, As and Kr doped ZnO films. There are two subroutines in SRIM main menu, “Stopping/Range Tables” and “TRIM calculations”. The first subroutine allows the rapid calculation of ion ranges over a large band of ion energies based on the transport equation approach. The latter is a Monte-Carlo calculation which follows the ion into the target, making detailed

calculations of the energy transferred to every target atom collision. In this paper, all our simulation results are based on "TRIM calculations". The threshold energies for atomic displacements of Zn and O atoms are set to be 34 eV and 44 eV, respectively, which were determined experimentally as the average over the direction-specific thresholds obtained within the 15^0 angular window for ZnO irradiation at 300 K [22].

We first simulated the distributions of implanted ions by using TRIM calculation. As examples, the distributions of multi-energy implanted ions for sample 3, sample 6 and sample 9 are shown in Fig.1. As can be seen, by using a sequence of four energy ion implantations, a total As implants range to about 280 nm in depth with a nearly even concentration of about 8×10^{19} /cm^3 from the film surface to about 150 nm in depth. For the multi-energy Kr doped ZnO, the implants range to about 120 nm in depth with a concentration of 5×10^{20} /cm^3 from 15 nm to 75 nm in depth. For the multi-energy Ar doped ZnO, the implants range to about 220 nm with a concentration of 5×10^{20} /cm^3 from 18 nm to 140 nm. The ion distribution profiles are similar to the sum of the individual Gaussian distributions for each implantation energy[11-13], where the projected range R_p (depth of the peak concentration) and longitudinal straggle ΔR_p at a certain energy were rapid calculated using the "Stopping/Range Tables" module in SRIM, and the ion distribution with implantation fluence Φ can be expressed as $N(x)=\frac{\Phi}{\Delta R_p\sqrt{2\pi}}\exp[-\frac{(x-R_p)^2}{2\Delta R_p{}^2}]$, where x is the depth from the surface. The latter method allows the rapid calculation of ion ranges over a large band of ion energies and is widely used to design the multi energy implantation parameters to give a desired ion distribution. The accuracy of ion ranges with the rapid method is usually within 5% of those found using TRIM, which is regard as the most accurate method of calculating ranges [18-21, 23].

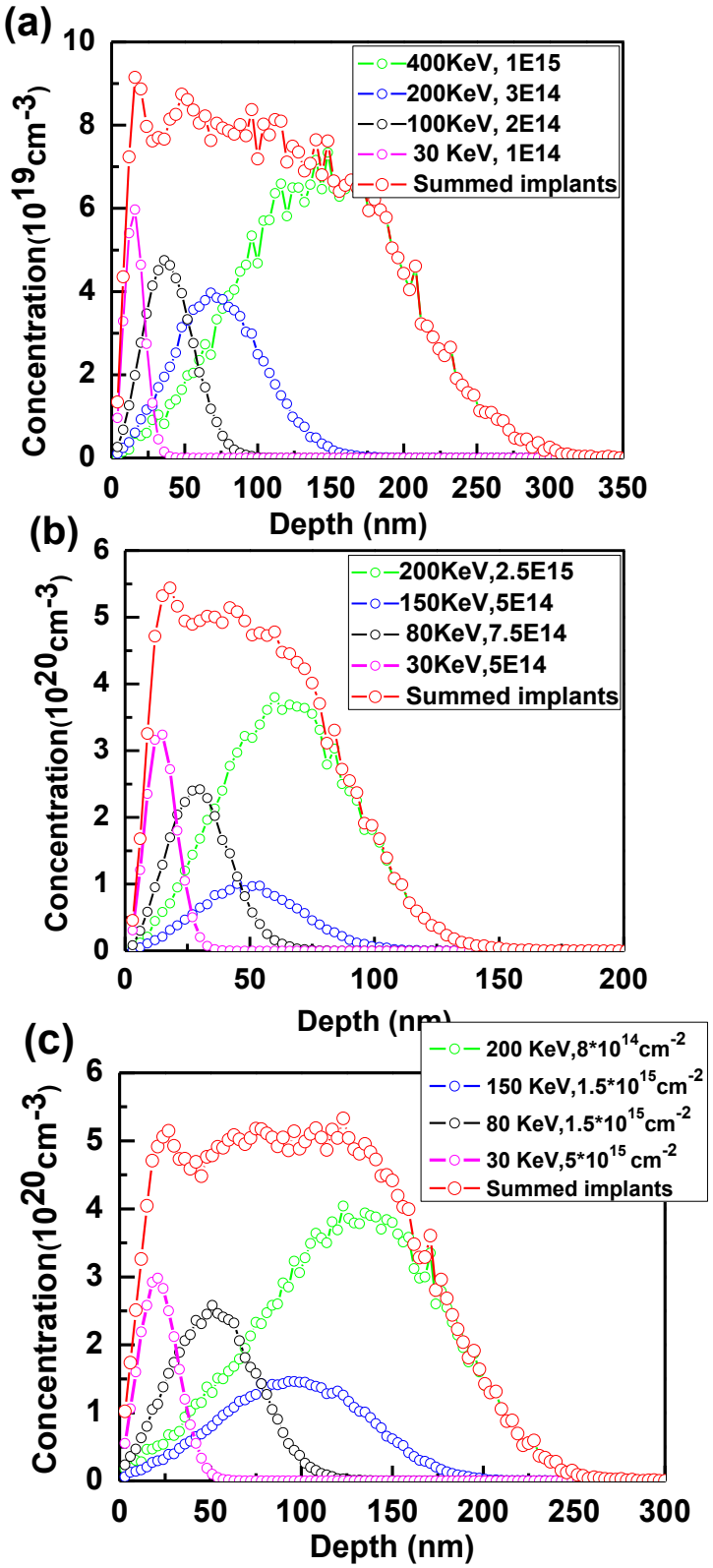

Fig. 1 (Color on line) (a) TRIM simulated As distribution in ZnO of sample 3; (b) TRIM simulated Kr distribution in ZnO of sample 6; (c) TRIM simulated Ar distribution in ZnO of sample 9.

The depth profiles of the summed Zn/O vacancies and interstitials for sample 3, sample 6 and sample 9 are shown in Fig.2. As can be seen, the depth distribution ranges of Zn/O vacancies and interstitials are similar to the implanted ion distributions shown in Fig.1, but the damage distributions are not as even as the ion distributions. For As doped ZnO, the damage peak is from 30 nm to 80 nm in depth, and for Kr and Ar doped films, they are from 20 to 40 nm and 30 to 70 nm, respectively. Our results show that the damage occurred as the implanted ions slowed down and hence was in a region that was closer to the sample surface than the average depth of the implanted ions. Also can be seen is that more Zn vacancies and interstitials are produced by implantation than O vacancies and interstitials, with a ratio of about 1.8, which may because of that the energy of a displaced Zn is lower than that of O, i.e., 34 eV versus 44 eV. The theoretical peak for the vacancy concentration is of order of 10^{23} vacancies/cm^3, which is unrealistic and occurs because SRIM simulates the primary radiation damage production and does not consider the recombination of the resultant vacancies and interstitials. It is believed that 99% of the Frenkel pairs recombine instantly, leaving only 1% damage [23]. Taking this into account, the peak vacancy density is estimated to be of the order of 10^{21} vacancies/cm^3. Structural characterization of the implanted film confirm that it is certainly damaged but the implanted layer is not amorphous, as would be for a vacancy concentration of 10^{23}cm^{-3}[11-13].

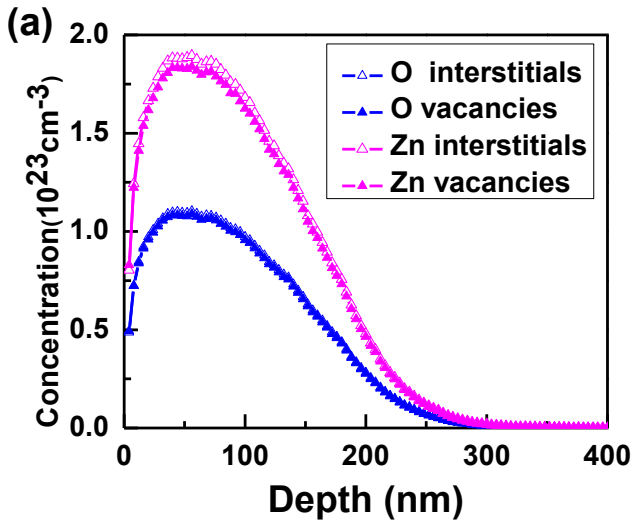

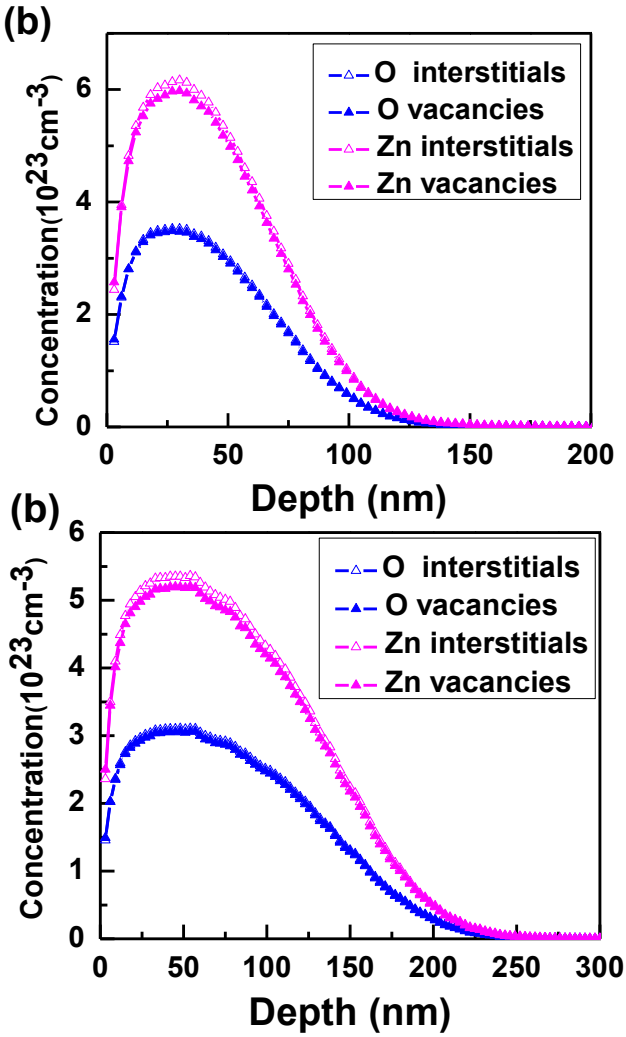

Fig. 3 (Color on line) SRIM simulated vacancy and interstitial distributions for (a)As doped-ZnO of sample 3; (b) Kr doped ZnO of sample 6; (c)Ar doped ZnO of sample 9

The radiation-damage effects due to different implantation conditions is compared using an analysis of the number of dpa which provides a common basis of comparison of the damage obtained due to different ions, As, Kr and Ar implanted at different energies.

The formula to calculate dpa in ion implantation is

$$\text{dpa} = \frac{\Phi(\text{ions/cm}^2)\times\gamma}{\text{N}} \qquad (1)$$

Where Φ is the implantation fluence, γ is the number of displacements produced by a primary knock-on atom (PKA), which can be found in the TRIM output file, and N is the atomic density, N= 8.3×10^{22} atoms/cm^3 for ZnO.

The number of displacements can also be calculated from the damage energy using

the internationally-recognized standard method, NRT model. According to NRT model, the total number of displacements produced by a PKA can be expressed as [24,25]:

$$\gamma = 0.8\frac{T_{dam}}{2E_d} \qquad (2)$$

Where T_{dam} is the damage energy and represents the portion of the PKA energy that is dissipated in elastic collisions with atoms in the lattice. With the lattice binding energy set to zero, the damage energy is simply the energy equal to the initial ion energy minus the energy dissipated in ionization [24]. For "TRIM calculations", there are two basic options named "Detailed Calculation with full Damage Cascades" and the "Ion Distribution and Quick Calculation of Damage", The first option is referred to as Full Cascade (F-C) and it follows every recoil until its energy drops below the lowest displacement energy of any target atom, hence all collisional damage to the target is included. The latter gives quick statistical estimates based on the Kinchin-Pease model, referred to as K-P option. Stoller et al. investigated the differences in calculating displacements by using the standard NRT model, SRIM-based displacement and MD calculation, and recommended that displacement from damage energy with K-P option is the best choice for dpa calculation by using SRIM simulation [24]. As their calculations based on iron and nickel target, to test the difference for ions implanted in compound semiconductors, calculations were carried out for ZnO implanted with As, Kr and Ar ions for a range of energies, as is shown in Table 2. It can be seen that the number of displacements per ions obtained from TRIM calculation with F-C option is much larger than that with K–P option, with a factor of about 1.5. However, the displacements calculated from damage energy with these two options are almost the same, with a ratio of 1.05-1.06. This is similar with the previous results of Fe ions implanted into pure iron and He ions implanted into nickel, where the larger factor is about 2 and the similar one is 1.05 to 1.1 [24]. In the following dpa calculation, we followed the recommendations given by the authors in Ref. [24], and calculated the displacement from damage energy with K-P option.

Fig.3 shows the depth dependence of dpa for sample 3, sample 6 and sample 9. As can be seen, sample 9 has a much broader dpa distribution with a maximum dpa value of 6.78 which is a little bit smaller than sample 6 but much bigger than sample 3. SQUID measurements show that considerable room temperature ferromagnetism has been observed for sample 3 and sample 6 while none for sample 9. It seems that

although magnetism originate from radiation damage for non-magnetic ions implanted ZnO films, magnetization is not solely determined by dpa and it also has a close relevance to the implanted ions itself.

Table 2 Damage calculations for sample 3, sample 6 and sample 9 using SRIM-2008.

Incident ion and energy (kev)	Calculation option in SRIM	Displacements from TRIM		Displacements from Damage energy	
		Integration of vacancy	F–C to K–P ratio	γ , Eq.(2)	F–C to K–P ratio
As, 400	F-C	371	1.49	248	1.05
	K-P	249		236	
As, 200	F-C	202	1.49	135	1.05
	K-P	135		128	
Kr, 200	F-C	199	1.50	133	1.06
	K-P	132		125	
Kr, 30	F-C	32	1.60	21	1.05
	K-P	20		20	
Ar, 200	F-C	157	1.47	106	1.03
	K-P	107		103	
Ar, 30	F-C	30	1.50	20	1.00
	K-P	20		10	

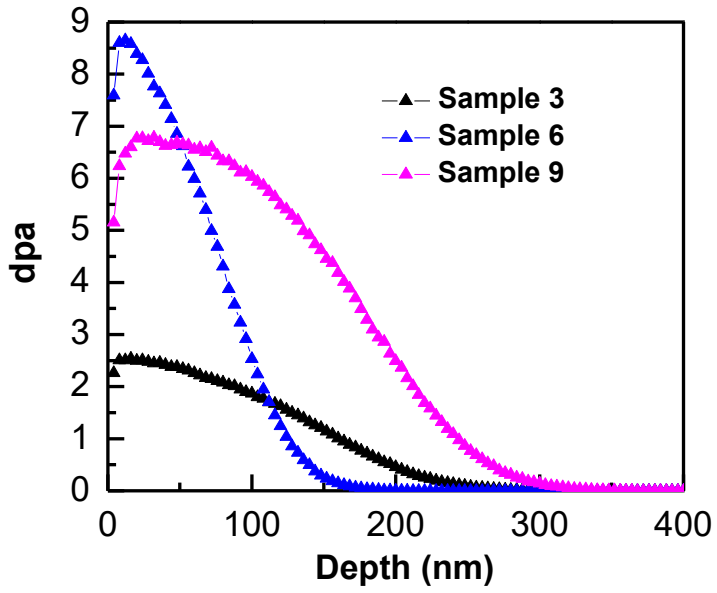

Fig.3 (Color on line) The depth dependence of dpa by SRIM simulation using K-P options with displacement obtained from damage energy for sample 3, sample 6 and sample 9.

To explore the effects of radiation damage on magnetism, Fig.4 shows the

dependence of saturation magnetization Ms at 5 K on the corresponding maximum dpa obtained from the in-depth profile in Fig.3. Linear fits of Ms versus dpa for each kind of ion implanted samples are also given. The linear fit occurs for samples that retain their crystallinity, as was found here, and should break down should the film become amorphous. A summary of damage and magnetization for sample at 5K were also given in Table 3. We used the values of the magnetization at 5K because the calculations of dpa performed by TRIM do not include temperature effects. As can be seen from Fig.4, ferromagnetism has been observed for krypton and arsenic implanted ZnO samples and the saturation magnetization increases with the increase of concentration of the implanted ions. ZnO samples doped with Ar have similar dpa with Kr but are not magnetic. It seems that Ms depends on the dpa for a given implanted ion but the constant of proportionality must depend on the mass or size of the implanted ion. Similar results have been obtained for ion implanted single crystalline $SrTiO_3$, where the authors showed that no relation between the occurring of ferromagnetism and the number of total atomic displacements introduced by implantation of different ions [26].

Our results proved that magnetization has a close relevance to the properties of implanted ions. Big magnetization can be realized for heavy ions implanted into ZnO films. This may because of that heavy ions might cause a marked grain fragmentation when implanted into the grains, leading to an increase in the volume of the sample occupied by grain boundaries. It has been shown that the grain boundaries that are produced as a result of ion implantation are more efficient at generating magnetism than point defects [13]. To obtain room temperature d^0 magnetism in ZnO, non-magnetic ions with high mass are suggested to be implanted into ZnO films.

Also it should be pointed out that SRIM simulates the primary radiation damage production and the subsequent reaction between the defects and the influence of ZnO surface polarity on damage and magnetism could not be considered here. Some of these defects can join up to give grain boundaries and this will certainly influence the resultant d^0 magnetism.

We can relate the observed magnetization, M_0, to the magnetization induced by each implanted ion, $q\mu_B$. For a fluence, Φ, over an area, A, the value of q is given by $q = \frac{M_0}{A\Phi\mu_B}$. The values found for samples 2,3,5,6 are 8, 14, 31,31 respectively. These numbers are too large to be associated with a single defect state associated with the

implanted ion and arise from the many defects formed as the implanted ions travels through the film.

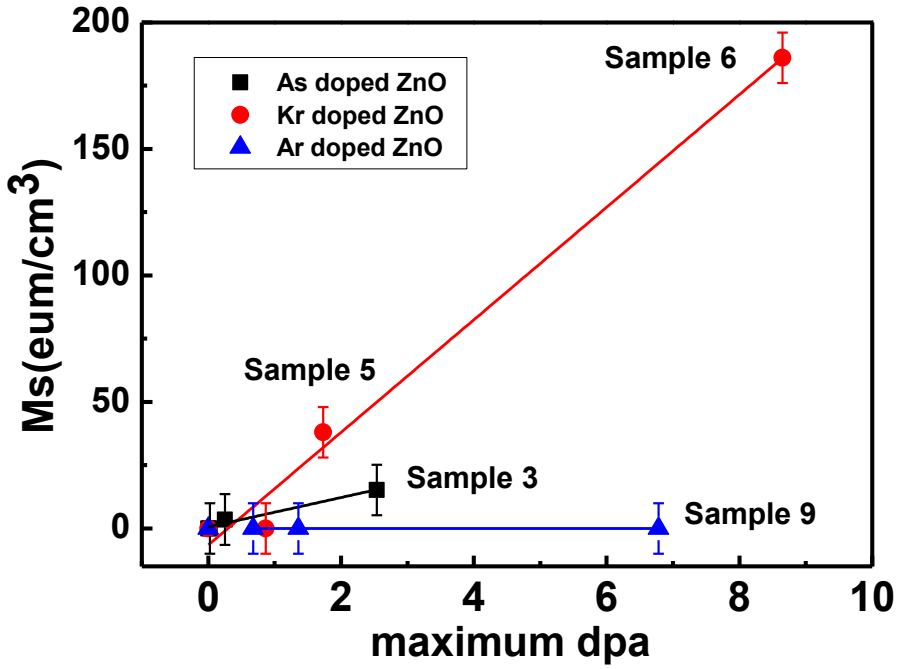

Fig. 5 **Ms vs the corresponding maximum dpa for sample 1 to 9 and the linear fits for each kind of ion implanted samples**

Table 3 Summary of the results for damage and magnetization for sample 3, sample 6 and sample 9

	Sample 3, As (75)	**Sample 6, Kr (84)**	**Sample 9, Ar (40)**
Concentration(cm^{-3})	8×10^{19}	50×10^{19}	50×10^{19}
Total fluence (cm^{-2})	16×10^{14}	42.5×10^{14}	98×10^{14}
Zn vacancies n_{Zn} (cm^{-3})	1.8×10^{23}	6×10^{23}	5.2×10^{23}
O vacancies n_o(cm^{-3})	1.2×10^{23}	3.5×10^{23}	3×10^{23}
Maximum dpa	2.5	8.7	6.7
M_s (T=5K) ($emu.cm^{-3}$)	15	186	~0

4. Conclusions

We have done the first systematic study of ion implantation in ZnO and its effects on magnetism. We used 3 different ions to implant into ZnO films deposited by rf-plasma assisted MBE. The magnetic properties of the samples were characterized by using a high sensitive SQUID. Considerable room temperature ferromagnetism has been observed for heavily As and Kr doped ZnO samples while not for Ar doped samples with similar damage distributions. Our results show that there is a strong dependence for magnetism on the type of ion as well as the ions concentration. The observed magnetic moment measured at low temperatures due to implantation with a given ion is proportional to the dpa. The constant of proportionality between the magnetism and the dpa depends on the implanted ion. This constant is largest for heavy, large ions. This may because of that heavy ions implanted into the grains might cause a marked grain fragmentation, leading to an increase in the volume of the sample occupied by grain boundaries. To obtain room temperature d^0 magnetism in ZnO, non-magnetic ions with high mass are suggested to be implanted into ZnO films. Although dpa is commonly used as a quantitative measure of radiation damage, and ion implantation induced d^0 magnetism is frequently observed experimentally, there is no previously published report on the relationship between the value of the dpa and the magnitude of magnetism in ion implanted ZnO films.

Acknowledgments

This work is financially supported by the National Natural Science Foundation of China under Grant No. 11875088 and 11675280. The measurements of SQUID were taken on apparatus initially funded by the UK Engineering and Physical Sciences Research EP/D070406/1.

Conflict of interest The authors declare that they have no conflict of interest.

References

[1] Ohno H (1998) Making nonmagnetic semiconductors ferromagnetic. Science 281:951–956.

[2] Dietl T, Ohno H, Matsukura F, Cibert J, Ferrand D (2000) Zener model description of ferromagnetism in zinc-blende magnetic semiconductors. Science 287:1019-1022.

[3] P. Sharma, A. Gupta, K. V. Rao, F. Owens, R. Sharma, R. Ahuja, J. Guillen, B. Johansson and G. A. Gehring (2003) Ferromagnetism above room temperature in bulk and transparent thin films of Mn-doped ZnO. Nature Mater 2:673-677.

[4] A.J. Behan, A. Mokhtari, H.J. Blythe, D. Score, X.H. Xu, J. R. Neal, A.M. Fox and G.A. Gehring (2008) Two Magnetic regimes in doped ZnO corresponding to a dilute magnetic semiconductor and a dilute magnetic insulator. Phys. Rev. Lett. 100:047206.

[5] F. Pan, C. Song, X. J. Liu, Y. C. Yang, F. Zeng (2008) Ferromagnetism and Possible Application in Spintronics of Transition-Metal-Doped ZnO Films. Mat. Sci. Eng. R 62:1-35.

[6] Minju Ying, Harry J. Blythe, Wala Dizayee, S.M. Heald, F.M. Gerriu, A.M. Fox and G.A. Gehring (2016) Advantageous use of metallic cobalt in the target for pulsed laser deposition of cobalt-doped ZnO films. Appl. Phys. Lett. 109: 072403.

[7] Shengqiang Zhou, Qingyu Xu (2008) Room temperature ferromagnetism in carbon-implanted ZnO. Appl. Phys. Lett. 93: 232507.

[8] K. Potzger, S. Zhou, J. Grenzer, M. Helm, J. Fassbender (2008) An easy mechanical way to create ferromagnetic defective ZnO. Appl. Phys. Lett. 92:182504.

[9] J. B. Yi, C. C. Lim, G. Z. Xing, H. M. Fan et al (2010) Ferromagnetism in dilute magnetic semiconductors through defect engineering: Li-doped ZnO. Phys. Rev. Lett. 104: 137201.

[10] Peng Zhan, Weipeng Wang, Can Liu, Yang Hu, Zhengcao Li et al (2012) Oxygen vacancy–induced ferromagnetism in un-doped ZnO thin films. J. Appl. Phys. 111: 033501.

[11] M.J. Ying, W. Cheng, X.X. Wang, B. Liao, X. Zhang, Z.X. Mei, X.L. Du, Heald, SM, H.J. Blythe, A.M. Fox, G.A. Gehring (2015) Surface-polarity-dependent ferromagnetism in arsenic-implanted ZnO films prepared by MBE. Materials Letter 144:12–14.

[12] Minju Ying, Shida Wang, Tao Duan, Bin Liao , Xu Zhang , Zengxia Mei, Xiaolong Du , F.M. Gerriu , A.M. Fox , G.A. Gehring (2016) The structure, optical and magnetic properties of arsenic implanted ZnO films prepared by molecular beam epitaxy. Materials Letters 171: 121–124.

[13] Minju Ying, Ahmad M.A. Saeedi, Miaomiao Yuan, Xia Zhang, Bin Liao, Xu Zhang, Zengxia Mei, Xiaolong Du, Steve M Heald, A. Mark Fox, Gillian A. Gehring (2019) Extremely large d^0 magnetism in krypton implanted polar ZnO films. Journal of Materials Chemistry C 7, 1138.

[14] S. Lautenschlaeger, J. Sann, N. Volbers, and B. K. Meyer, A. Hoffmann, U. Haboeck, and M.

R. Wagner (2008) Asymmetry in the excitonic recombinations and impurity incorporation of the two polar faces of homoepitaxially grown ZnO films. Phys. Rev. B 77: 144108.

[15] Shengqiang Zhou (2014) Defect-induced ferromagnetism in semiconductors: A controllable approach by particle irradiation. Nuclear Instruments and Methods in Physics Research B 326 :55–60.

[16] Peng Zhan, Zheng Xie, Zhengcao Li, Weipeng Wang, Zhengjun Zhang, Zhuoxin Li, Guodong Cheng, Peng Zhang, Baoyi Wang, and Xingzhong Cao (2013) Origin of the defects-induced ferromagnetism in un-doped ZnO single crystals. Appl. Phys. Let. 102: 071914.

[17] KayPotzger (2012) Ion-beam synthesis of magnetic semiconductors. Nucl. Instrum. Meth. B. 272 : 78-87.

[18] J.F. Ziegler, J. Biersack, U. Littmark (1985) The Stopping and Range of Ions in Matter. Pergamon Press, New York.

[19] J.F. Ziegler (2004) SRIM-2003.Nucl. Instr. Meth. Phys. Res. Sect. B 219:1027-1036.

[20] J.F. Ziegler, J.P. Biersack, M.D. Ziegler (2008) SRIM –The Stopping Range of Ions in Matter. Cadence Design Systems.

[21] J.F. Ziegler, M.D. Ziegler, J.P. Biersak (2010) SRIM –The stopping and range of ions in matter. Nucl. Instr. Meth. Phys. Res.Sect. B 268: 1818-1823.

[22] D. C. Look, G. C. Farlow, Pakpoom Reunchan, Sukit Limpijumnong, S. B. Zhang, and K. Nordlund (2005) Evidence for Native-Defect Donors in n-Type ZnO. Phys. Rev. Lett. 95: 225502.

[23] J. F. Ziegler. SRIM-Lessons and Tutorials http://www.srim.org/SRIM/Tutorials

[24] R.E. Stoller, M.B. Toloczko, G.S. Was, A.G. Certain, S. Dwaraknath, F.A. Garner (2013) On the use of SRIM for computing radiation damage exposure. Nuclear Instruments and Methods in Physics Research B 310 : 75–80.

[25] M.J. Norgett, M.T. Robinson, I.M. Torrens (1975) A Proposed Method of Calculating Displacement Dose Rates. Nuclear Engineering and Design 33:50-54.

[26] K. Potzger, J. Osten, A.A. Levin, A. Shalimov, G. Talut, H. Reuther, S. Arpaci, D. Burger, H. Schmidt, T. Nestler, D.C. Meyer (2011) Defect-induced ferromagnetism in crystalline SrTiO3. J. Mag. Mag. Mater. 323: 1551–1562